CHINESE OPTICS LETTERS

Vol. 22, No. 1 | January 2024

Terahertz spectroscopy of water in nonionic reverse micelles

Jiaqi Zhang (张佳琦)[1], Yuyue Yan (闫玉岳)[1], Liyuan Liu (刘立媛)[1*], and Weili Zhang (张伟力)[2**]

[1] Centre for Terahertz Waves and College of Precision Instrument and Optoeletronics Engineering, Tianjin University, Tianjin 300072, China

[2] School of Electrical and Computer Engineering, Oklahoma State University, Stillwater, Oklahoma 74078, United States

*Corresponding author: lyliuma@tju.edu.cn

**Corresponding author: weili.zhang@okstate.edu

Received May 31, 2023 | Accepted August 15, 2023 | Posted Online January 8, 2024

The dynamics of water within a nanopool of a reverse micelle is heavily affected by the amphiphilic interface. In this work, the terahertz (THz) spectra of cyclohexane/Igepal/water nonionic reverse micelle mixture are measured by THz time-domain spectroscopy and analyzed with two Debye models and complex permittivity of background with volume ratios. Based on the fitted parameters of bulk and fast water, the molar concentration of all kinds of water molecules and hydration water molecule number per Igepal molecule are calculated. We find that slow hydration water has the highest proportion in water when the radius parameter $\omega_0 < 10$, while bulk water becomes the main component when $\omega_0 \geq 10$. The feature radius ratio of nonhydrated and hydrated water to total water nanopool is roughly obtained from 0.39 to 0.85 with increasing ω_0.

Keywords: reverse micelle; water dynamics; THz spectroscopy.

DOI: 10.3788/COL202422.013001

1. Introduction

Water is the source of life. Interactions between water and amphipathic substances play significant roles in many fundamental biochemical and physical processes, such as the operation of biofilm[1,2] and salting-out effects of proteins[3]. A common example is that soap relies on the amphiphilic characteristics of the soap compound to make water easier to wash hydrophobic dirt off. The dynamics of water around amphiphilic compounds is a key question for understanding these common biochemical and physical phenomena. However, the question "how does interaction with the interface of amphiphilic compound change the dynamics of water ?" has not been answered clearly yet[4,5].

When water is added into a mixture with surfactant and organic solvent, nanometer-scale pools will be formed in a mixture in which water molecules are wrapped around the polar interface of the surfactant. The reorientation processes of water molecules near the interface of the surfactant are affected by the amphiphilic interface and become different with water molecules located in the center of a nanopool. The dynamics of water within a confined environment has been widely studied in the last few decades with various technologies, such as terahertz (THz) dielectric relaxation spectroscopy[6,7], IR pump probe[8,9], FT-IR spectroscopy[10], X-ray diffraction (XRD)[11], 2D infrared vibrational spectroscopy[12], and membrane distillation (MD) simulation[13]. Most of these techniques utilize the relationship between electromagnetic wave and intermolecular or intramolecular dipoles of water molecule to obtain dynamic information of water. Specially, THz dielectric spectroscopy can provide an intermolecular dielectric response with a time scale of 10^{-12} seconds and probe the first-order correlation function of water molecular dipoles.

Aerosol-OT (AOT) and Igepal CO-520 are common surfactants that are often used to prepare ionic or nonionic reverse micelle nanopools with a certain size (~1 nm to ~10 nm). Many nanometer particles have been synthesized successfully within predesigned reverse micelle nanopools for a variety of novel applications, such as nanofluids[14], fluorescent bioassays[15], delivery of hydrophilic drugs[16], and food applications[17]. Compared with the ionic reverse micelle, the nonionic reverse micelle is more convenient for analysis of dynamics of water at the interface of the surfactant because of the simple amphiphilic ends of the surfactant molecules without consideration of the effect of ions.

THz is the electromagnetic wave ranging from 0.1 to 10 THz. Recently, because of wonderful properties such as low photon energy, higher frequency than microwaves, and ideal security, the THz wave has been widely applied in various fields such as disease detection[18,19], security detection[20,21], 6G high-speed

wireless communication[22,23], and analysis of the mechanism of matter[24]. In particular, the THz wave coincides with the frequency of the rotational mode of water molecules in hydrogen bond networks, which provides the fundament for the study of the rotational dynamics of water using THz.

In this work, cyclohexane/Igepal CO-520/water reverse micelle mixtures are prepared to study the reorientation relaxation dynamics of water molecules with THz spectroscopy from 0.5 to 2 THz. Two Debye models and complex permittivity of background with volume ratios are used to describe the dielectric relaxation of reverse micelles. Based on the relaxation strengths of fast and bulk water, the amounts of fast water, bulk water, and slow hydration water (which is a water molecule at the interface between Igepal and a water nanopool) are calculated. Furthermore, the radius ratio of nonhydrated and hydrated water to the total nanopool also has been estimated.

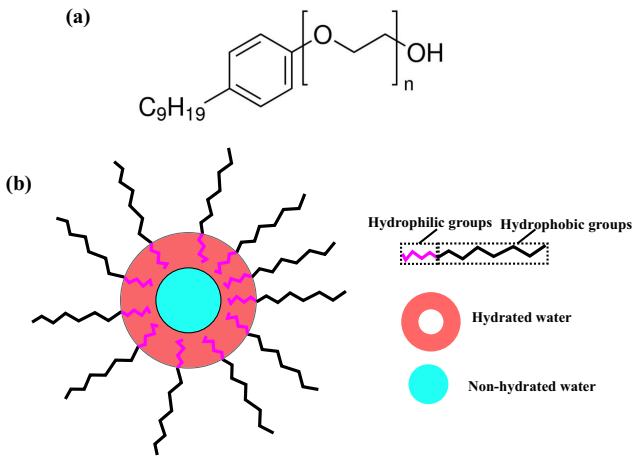

Fig. 1. (a) Molecular formula of Igepal CO-520; n in the formula is about 5. (b) Schematic illustration of prepared reverse micelle.

2. Experiment

2.1. Sample preparation

Nonionic reverse micelles are prepared with pure water/Igepal CO-520 [polyoxyethylene (5) nonylphenylether, branched, $M_n \simeq 441$]/cyclohexane ternary liquid system. The water, Igepal, and cyclohexane were purchased from Sigma Aldrich. The pure water was purified by the Millipore system and has a resistivity of 18.2 MΩ cm. The molecular formula of Igepal and the schematic structure of prepared nonionic reverse micelles are shown in Fig. 1. The water nanopool consists of two parts: hydrated water that gets close to the hydrophilic groups of Igepal and nonhydrated water which is distributed in the center of the nanopool. The hydrophobic ends of Igepal are in contact with cyclohexane. The radius r of nanopools of reverse micelles is determined linearly with parameters ω_0 defined as follows:

$$r = a\omega_0, \tag{1}$$

where a is a proportionality that is relevant to the type of surfactant, and ω_0 can be calculated by

$$\omega_0 = \frac{[H_2O]}{[\text{Igepal}]}, \tag{2}$$

where operator $[\cdot]$ represents the amount of the substance within brackets. Seven reverse micelle samples with $\omega_0 = 0$, 1.5, 3, 5, 8, 10, and 15 have been prepared, as shown in Table 1.

Table 1. Quantities of Chemical Compound Components in Prepared Reverse Micelles.

ω_0	0	1.5	3	5	8	10	15
Water/g	0	0.12	0.24	0.4	0.64	0.8	1.2
Igepal/g	2	2	2	2	2	2	2
Cyclohexane/g	5	5	5	5	5	5	5

2.2. THz measurement

The THz spectra from 0.5 to 2 THz were measured by THz time-domain spectroscopy (THz-TDS). In the 8-F THz time-domain confocal system, the THz radiation is emitted from a GaAs substrate photoconductive antenna that is excited by an 800 nm Mantis laser (Coherent Inc.) with a duration of 50 fs and repetition rate of 80 MHz. A square wave (AC voltage of 70 V) is applied on the parallel gold nanoelectrode to accelerate photon-excited free electrons. Another GaAs substrate antenna without external voltage is used as a receiver in which the photon-excited free carriers are directly driven by the THz wave. In the receiver terminal, a delay line was deployed to detect light current at different times. The output light current is proportional to the strength of the THz field. A more detailed introduction of the time-domain system is available in other sources[25].

The samples to be measured were put into a quartz glass sample cell with a light path of 1 mm. The complex THz permittivity of one sample was obtained by series of calculations based on a reference sample cell with air and a sample cell filled with prepared mixture[26]. The final results of the complex permittivity of the samples were averaged from measuring the samples three times. All measurements proceeded at room temperature and at a relative humidity lower than 3%. The time and frequency domain spectra of transmitted THz signals are shown in Fig. 2. We can see there are some waves in the frequency domain signal of air reference, which are caused by the second reflection of THz waves of air reference, as we can see the small time-domain peak in the time-domain spectrum. In the follow-up calculation of complex permittivity, the second reflections of the time-domain signal are cut off.

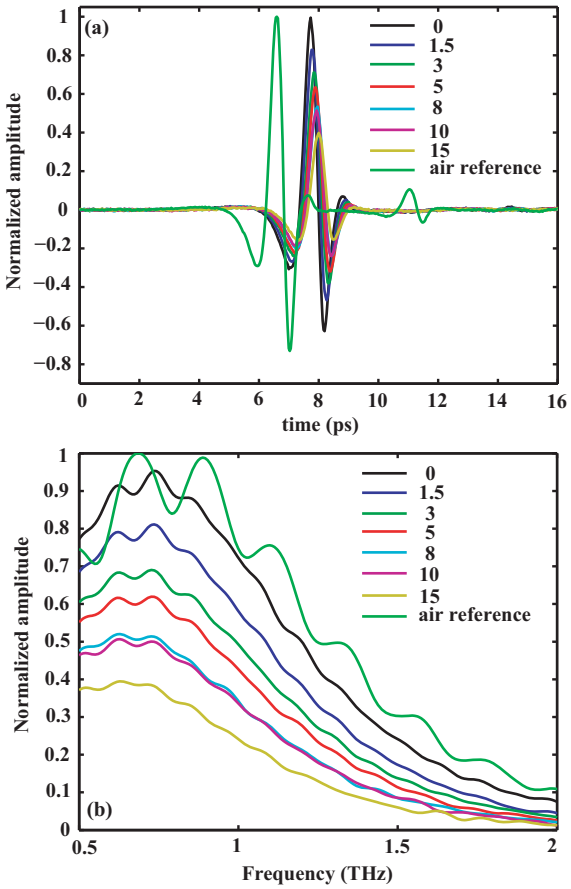

Fig. 2. (a) Time-domain spectra of air reference and measured reverse micelle mixtures; (b) frequency-domain spectra of air reference and measured reverse micelle mixtures.

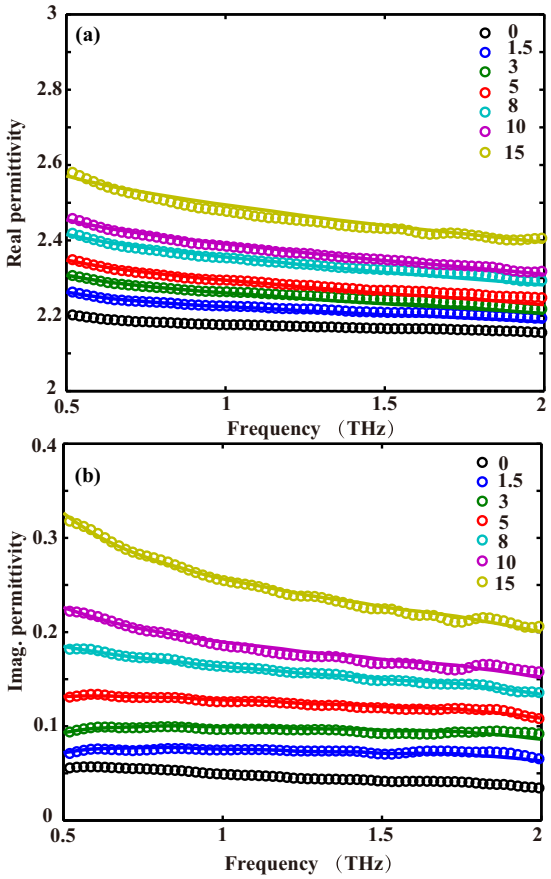

Fig. 3. THz complex permittivity (circle markers) of reverse micelles and fitted lines (solid lines) with proposed model.

3. Results and Analysis

In the pure water, there are only two types of water molecules in wate: fast water (water molecules are not involved in a hydrogen bond network or are involved in fewer hydrogen bonds) and bulk water (water in the tetrahedral hydrogen bond network). The rotational dynamics from gigahertz (GHz) to THz of water molecules can be described by two Debye models as follows[27,28]:

$$\hat{\varepsilon}(\omega) = \frac{S_{\text{fast}}}{1 + i\omega\tau_{\text{fast}}} + \frac{S_{\text{bulk}}}{1 + i\omega\tau_{\text{bulk}}} + \varepsilon_{\infty}, \tag{3}$$

where the first and second terms represent the reorientation relaxation of fast water and bulk water, respectively, S_{fast} and S_{bulk} are the relaxation strength of fast and bulk water, respectively, τ_{fast} and τ_{bulk} are the relaxation time of fast and bulk water, respectively, and the ε_{∞} is the high-frequency limit permittivity. While there are some amphiphilic groups in reverse micelle solutions, the fast and bulk water will be affected by these groups (hydrophilic effects from hydroxy and ether groups and hydrophobic effect) via strong hydrogen bonds, and some of them transform into slow hydration water with slower reorientation rotation. In this system, the dynamics of water from GHz to THz generally can be described as multiple Debye models[29,30],

$$\hat{\varepsilon}(\omega) = \frac{S_{\text{fast}}}{1 + i\omega\tau_{\text{fast}}} + \frac{S_{\text{bulk}}}{1 + i\omega\tau_{\text{bulk}}} + \sum_{n} \frac{S_n}{1 + i\omega\tau_n} + \varepsilon_{\infty}, \tag{4}$$

where the first two terms are the relaxation processes of fast and bulk water, respectively, the multiple dependent Debye modes in the third term are the process of slow hydration water, which is mainly distributed around the interface of Igepal, as shown by the red region in Fig. 1, and S_n and τ_n are the relaxation strength and time of the nth slow hydration water, respectively. The relaxation peak of slow hydration water is generally distributed at a frequency lower that 10 GHz, which implies that the imaginary parts of the complex permittivity of the slow hydration approach 0 in the THz region; that is to say, the dielectric relaxation of water in the THz region basically excludes the contribution of slow hydration water. While we can see the complex permittivity of $\omega_0 = 0$ in the reverse micelle in Fig. 3, the imaginary part is not equal to 0 and has the same order of magnitude as the complex permittivity of reverse micelle mixtures. In GHz and THz dielectric spectroscopy, compared with the permittivity of water, the permittivity of the background is too small and can be neglected[30]. While only in the THz region, the value of

Table 2. Relevant and Fitted Parameters from Eq. (5).

ω_0	S_{fast}	S_{bulk}	ε_∞	f
1.5	0.06	0	0.04	0.98
3	0.10	0.26	0.07	0.97
5	0.14	1.06	0.12	0.95
8	0.16	2.28	0.22	0.93
10	0.18	3.26	0.28	0.91
15	0.24	5.54	0.42	0.87

the permittivity of the reverse micelles is comparable with water in reverse micelles within a small nanopool. Therefore, we could describe the dielectric relaxation of the reverse micelle solution with the consideration of background (Igepal and cyclohexane) as follows:

$$\hat{\varepsilon}(\omega) = \frac{S_{fast}}{1 + i\omega\tau_{fast}} + \frac{S_{bulk}}{1 + i\omega\tau_{bulk}} + f\hat{\varepsilon}_{back}(\omega) + \varepsilon_\infty, \quad (5)$$

where f is the proportion of Igepal and cyclohexane in the reverse micelle mixture, and $\hat{\varepsilon}_{back}(\omega)$ represents the complex permittivity of the background in the third term. In order to restrict the number of free parameters, we reasonably fix τ_{fast} and τ_{bulk} for fast (0.1 ps) and bulk water (8.4 ps), respectively[30,31]. The measured complex permittivity and fitted lines of samples are shown in Fig. 3. We can see clearly the fitted lines match well with measured data.

The relevant and obtained parameters from fitting can be seen in Table 2. Intuitively, S_{fast}, S_{bulk}, and ε_∞ gradually become larger with ω_0 because more water with more apparent dielectric property in the THz region is added into the reverse micelle mixtures. An interesting thing is that S_{bulk} is equal to 0 when $\omega_0 = 1.5$, that is to say, there is almost no bulk water but only fast water and slow hydration water in reverse micelles. This makes sense because the nanopool is too tiny to support bulk water within it. A work[32] reported that there are about 40 water molecules in a $\omega_0 = 2$ AOT reverse micelle nanopool. Affected by the amphiphilic interface of Igepal, most of the little bulk water is easy to convert into slow hydration water or fast water. The trend of ε_∞ with the addition of water is also seen because the high frequency mainly comes from water in this ternary system, which can be judged from the small real part of the permittivity of the $\omega_0 = 0$ mixture with no dispersion, as the black circle markers show in Fig. 3(a).

To observe the dynamics of each component clearly, Fig. 4 shows the decomposed spectra of $\omega_0 = 5$ and 15 reverse micelles based on Eq. (5). The blue curve indicates the fast water with $\tau_{fast} = 0.1$ ps, whose relaxation peak is located at 1.55 THz, the green curve represents the dielectric relaxation of bulk water in the THz region, whose relaxation peak is distributed at 18.9 GHz, and the pink curve is the dielectric information of

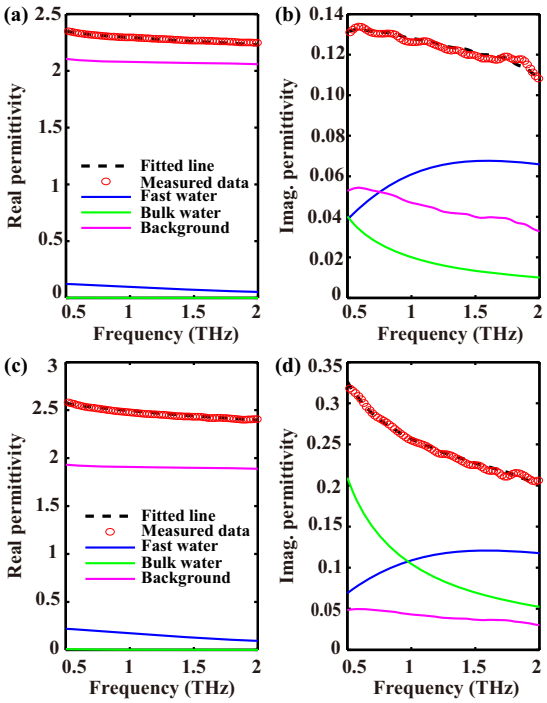

Fig. 4. Decomposed spectra of (a)–(b) $\omega_0 = 5$ and (c)–(d) 15 including fast water (blue solid line), bulk water (green solid line), and the background, which is determined linearly by the permittivity of $\omega_0 = 0$ mixture (pink solid line). (a), (c) and (b), (d) represent the real and imaginary part of obtained complex permittivity, respectively. The black dashed line is the fitted line with the proposed model.

the background in solution. Obviously, the contributions to total permittivity from water become larger with increasing ω_0.

Although the dielectric loss in the THz region is basically due to no contribution of slow hydration water, this does not prove that there is no slow hydration water in water. With the relationship between the relaxation strength of pure water and the sum of the relaxation strengths of fast and bulk water in reverse micelles, we could determine that there is slow hydration water in water and calculate the molar concentration of each water component. The molar concentration of fast and bulk water can be calculated by[33,34]

$$c_i(\omega_0) = \frac{S_i(\omega_0)/g_i(\omega_0)}{S_{fast,pure}/g_{fast}(0) + S_{bulk,pure}/g_{bulk}(0)} c_{H_2O}(0), \quad (6)$$

where subscript i can be fast and bulk water, $S_i(\omega_0)$ represents the relaxation strength of the fast and bulk water in ω_0 reverse micelle, $g_i(\omega_0)$ represents the Kirkwood factor of fast and bulk water in ω_0 reverse micelle mixture, and $g_{fast}(0)$ and $g_{bulk}(0)$ are the Kirkwood factor of fast and bulk water in pure water, respectively. $S_{fast,pure}$ and $S_{bulk,pure}$ are the relaxation strength of fast and bulk water in pure water, respectively, and $c_{H_2O}(0)$ is the molar concentration of pure water, which is 55 mol/L. Here, we set $S_{fast,pure} = 3.5$ and $S_{bulk,pure} = 72.2$, which are calculated

from the pure water in the GHz and THz regions with two Debye models[30].

We assume that the Kirkwood factor of fast water in pure water and overall reverse micelle mixture is equal to 1, which is the same as the bulk water in the overall calculations. The Kirkwood factor represents the observable mean square molecular dipole moment, which means that fast water and bulk water have same mean square molecular dipole moment in our assumption. Then the molar concentration of slow hydration water component can be obtained by the following equation:

$$c_{\text{slow}}(\omega_0) = c_{\text{H}_2\text{O}}(\omega_0) - \frac{S_{\text{fast}}(\omega_0) + S_{\text{bulk}}(\omega_0)}{S_{\text{fast,pure}} + S_{\text{bulk,pure}}} c_{\text{H}_2\text{O}}(0), \quad (7)$$

where $c_{\text{H}_2\text{O}}(\omega_0)$ represents the molar concentration of water in ω_0 mixture and can be obtained by simply multiplying the volume ratio of water to the ω_0 total reverse micelle mixtures by the molar concentration of pure water.

Based on Eqs. (6) and (7), the molar concentration is obtained and shown in Fig. 5(a). Here, the black line represents the molar concentration of pure water in ω_0 reverse micelle solution, which shows a trend of direct proportional growth with the increasing size of the nanopool. The blue, green, and red curves show the molar concentration of fast, bulk, and slow hydration water, respectively. We can see that the water with the least amount is always fast water except $\omega_0 = 1.5$. With the addition of water, the amount of all types of water keeps rising with increasing ω_0, the amounts of bulk water and fast water basically keep linear growth from $\omega_0 = 3$ to 15, while the growth rate of the amount of hydrated water slows down and is lower than that of bulk water.

The hydration water number per Igepal molecule also can be obtained by dividing the concentration of water by the concentration of Igepal in ω_0 reverse micelle. Figure 5(b) shows that the hydration water number per Igepal molecule increases from 1.4 to 5.6. There are six hydrophilic groups in an Igepal molecule: five ether groups and one hydroxy group, which is the closest group to the water molecule in the nanopool. The hydration water number per Igepal molecule implies that not every hydrophilic group is in contact with a hydration water molecule when ω_0 is a small value. When $\omega_0 = 1.5$, 1.4 water molecules are most likely hydrogen-bonded to hydroxyl groups because the hydroxyl groups are the closest to the water nanopool. With the increase of ω_0, the hydration water may be hydrogen-bonded to ether groups. When ω_0 is less than 15, not all ether groups are attached to water molecule with a hydrogen bond because the hydration water number per Igepal molecule is always less than 6, which is less than the number of hydrogen bonding sites at hydrophilic groups of one Igepal molecule.

For simplicity, we assume that the nanopool in a reverse micelle is composed of nonhydrated and hydrated water, as shown in Fig. 6(a). Based on the amount of nonhydrated water (fast and bulk water) and slow hydration water, we can roughly calculate the feature radius ratio of nonhydrated and hydrated water to the total water nanopool by the following equations:

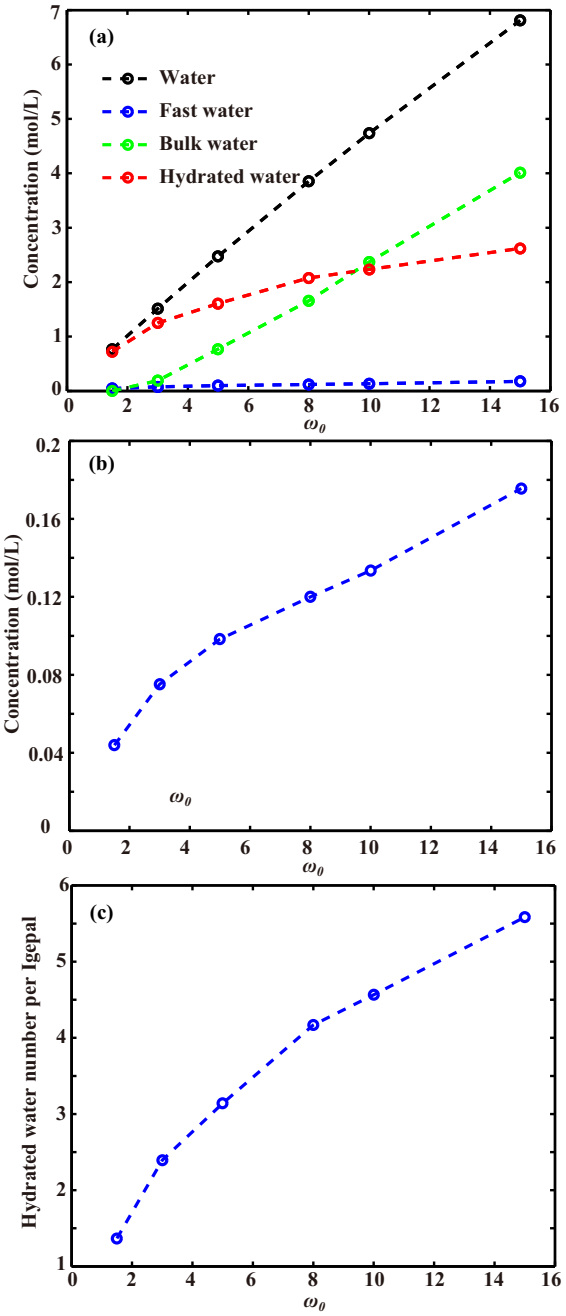

Fig. 5. (a) Obtained molar concentration of fast water (blue dashed line), bulk water (green dashed line), hydration water (red dashed line), and total water (black dashed line); (b) zoomed-in molar concentration of fast water; (c) calculated hydration water number per Igepal molecule.

$$\frac{r_{\text{Non-hydrated}}(\omega_0)}{r_{\text{water}}(\omega_0)} = \sqrt[3]{\frac{N_{\text{Non-hydrated}}(\omega_0)}{N_{\text{water}}(\omega_0)}}, \quad (8)$$

$$\frac{r_{\text{Hydrated}}(\omega_0)}{r_{\text{water}}(\omega_0)} = 1 - \frac{r_{\text{Non-hydrated}}(\omega_0)}{r_{\text{water}}(\omega_0)}, \quad (9)$$

where $r_{\text{Non-hydrated}}$ and r_{Hydrated} represent the radius of nonhydrated and hydrated water, respectively, r_{water} is the radius of

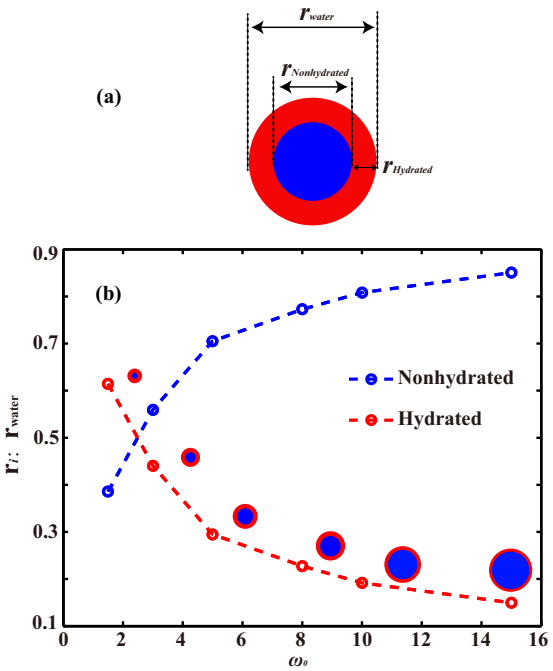

Fig. 6. (a) Definition of radius of nonhydrated, hydrated, and the total water nanopool; (b) ratios of the radius of nonhydrated (blue circles and dashed line) and hydrated water (red circles and dashed line) to the radius of the total water nanopool.

the total nanopool, $N_{\text{Non-hydrated}}$, N_{Hydrated}, and N_{water} represent the amount of nonhydrated water, hydrated water, and the total amount of water in the nanopool, respectively. The results of the radius ratio can be seen in Fig. 6(b). Obviously, the blue curve shows that the radius ratio of nonhydrated water to total water gradually increases, and the growth rate slows down with the increase of ω_0. In turn, the red curve shows that the radius ratio of hydrated water to the total nanopool gradually decreases, and the rate of decline gradually slows down with ω_0. The actual radius of hydration water can be obtained from the radius ratio of hydrated water to total water based on

$$r_{\text{Hydrated}} = a\omega_0 \frac{r_{\text{Hydrated}}(\omega_0)}{r_{\text{water}}(\omega_0)}. \tag{10}$$

Based on the above formula, r_{Hydrated}/a can be obtained as 0.92, 1.32, 1.47, 1.82, 1.92, and 2.23. Although the radius ratio of hydrated water to the total water nanopool is decreasing, the actual radius of hydrated water gradually increases with the growth of ω_0. It symbolizes the expansion of the nanopool with the addition of water.

4. Conclusion

In this work, the complex permittivities of cyclohexane/Igepal/water nonionic reverse micelles with $\omega_0 = 0$, 1.5, 3, 5, 8, 10, and 15 are analyzed using THz spectroscopy. The two Debye models with fast water, bulk water, and dielectric relaxations of the background are used to describe the complex permittivity of the prepared reverse micelles. The relaxation strengths of fast and bulk water in ω_0 reverse micelle are calculated from the proposed model. The molar concentrations of fast, bulk, and hydration water are next estimated. Interestingly, in the $\omega_0 = 1.5$ reverse micelle mixture, there is almost no bulk water, but only fast and hydration water, while the molar concentration of bulk water grows linearly from $\omega_0 = 3$ to 15. The hydrated water number per Igepal molecule from 1.4 to 5.6 is obtained and shows the distribution geography of water molecule at the interface. When $\omega_0 = 0$, 1.5 water molecules are more likely to hydrogen-bond to the hydroxy group, which is the closest to the water nanopool. From the amount of each component of water, the radius ratios of nonhydrated and hydrated water to the total nanopool are also estimated, where the ratios of nonhydrated water increase from 0.38 to 0.85, and those of hydrated water decrease from 0.61 to 0.15. Furthermore, the radius of hydrated water gradually increases with ω_0, while the growth rates of the radius of hydrated water gradually slow down. This indicates the expansion of the water nanopool and its morphologic change.

Acknowledgements

This work was supported by the National Natural Science Foundation of China (No. 62175185).

References

1. N. Yamamoto, S. Ito, M. Nakanishi, *et al.*, "Effect of temperature and hydration level on purple membrane dynamics studied using broadband dielectric spectroscopy from sub-GHz to THz regions," J. Phys. Chem. B **122**, 1367 (2018).
2. Z. W. Ding, L. Y. Liu, Z. M. Li, *et al.*, "Experimental study of ammonia removal from water by membrane distillation (MD): the comparison of three configurations," J. Membr. Sci. **286**, 93 (2006).
3. B. A. Rogers, H. I. Okur, C. Y. Yan, *et al.*, "Weakly hydrated anions bind to polymers but not monomers in aqueous solutions," Nat. Chem. **14**, 40 (2022).
4. Y. L. A. Rezus and H. J. Bakker, "Observation of immobilized water molecules around hydrophobic groups," Phys. Rev. Lett. **99**, 148301 (2007).
5. W. H. Brandeburgo, S. T. van der Post, E. J. Meijer, *et al.*, "On the slowdown mechanism of water dynamics around small amphiphiles," Phys. Chem. Chem. Phys. **17**, 24968 (2015).
6. A. Patra, T. Q. R. K. Mitra, and M. Havenith, "The influence of charge on the structure and dynamics of water encapsulated in reverse micelles," Phys. Chem. Chem. Phys. **16**, 12875 (2014).
7. M. Schmollngruber, D. Branun, and O. Steinhauser, "A computational component analysis of dielectric relaxation and THz spectra of water/AOT reverse micelles with different water loading," J. Chem. Phys. **145**, 214702 (2016).
8. S. Park, D. E. Moilanen, and M. D. Fayer, "Water dynamics-the effects of ions and nanoconfinement," J. Phys. Chem. B **112**, 5279 (2008).
9. H. Tan, I. R. Piletic, R. E. Riter, *et al.*, "Dynamics of water confined on a nanometer length scale in reverse micelles: ultrafast infrared vibrational echo spectroscopy," Phy. Rev. Lett. **94**, 057405 (2005).
10. A. Sengupta, R. V. Khade, and P. Hazra, "How does the urea dynamics differ from water dynamics inside the reverse micelle?" J. Phys. Chem. A **115**, 10398 (2011).
11. T. H. Loop, M. R. Panman, S. Lotze, *et al.*, "Structure and dynamics of water in nonionic reverse micelles: a combined time-resolved infrared and small angle X-ray scattering study," J. Chem. Phys. **137**, 044503 (2012).

12. V. V. Volkov, D. J. Palmer, and R. Righini, "Distinct water species confined at the interface of a phospholipid membrane," Phys. Rev. Lett. **99**, 078302 (2007).
13. M. Crowder, F. Tahiry, I. Lizarraga, *et al.*, "Computational analysis of water dynamics in AOT reverse micelles," J. Mol. Liq. **375**, 121340 (2023).
14. P. Zhang, D. Shen, A. T. Kana, *et al.*, "Synthesis and laboratory testing of a novel calcium-phosphonate reverse micelle nanofluid for oilfield mineral scale control," RCS Adv. **6**, 39883 (2016).
15. T. Osaka, T. Matsunaga, T. Nakanishi, *et al.*, "Synthesis of magnetic nanoparticles and their application to bioassays," Analy. Bio. Chem. **384**, 593 (2006).
16. S. J. Myung, H. Kim, Y. Kim, *et al.*, "Fluorescent silk fibroin nanoparticles prepared using a reverse microemulsion," Macromol. Res. **16**, 604 (2008).
17. M. D. Chatzidaki, K. Papadimitriou, V. Alexandraki, *et al.*, "Reverse micelles as nanocarriers of nisin against foodborne pathogens," Food Chem. **255**, 97 (2018).
18. Y. Peng, J. L. Huang, J. Luo, *et al.*, "Three-step one-way model in terahertz biomedical detection," PhotoniX **2**, 12 (2021).
19. H. Lindley-Hatcher, R. I. Stantchev, X. Chen, *et al.*, "Real time THz imaging-opportunities and challenges for skin cancer detection," Appl. Phys. Lett. **118**, 230501 (2021).
20. X. Yang, T. Wu, L. Zhang, *et al.*, "CNN with spatio-temporal information for fast suspicious object detection and recognition in THz security images," Signal Pro. **160**, 202 (2019).
21. L. Cheng, Y. C. Ji, C. Li, *et al.*, "Improved SSD network for fast concealed object detection and recognition in passive terahertz security images," Sci. Rep. **12**, 12082 (2022).
22. H. W. Oleiwi, N. Saeed, and H. Al-Raweshidy, "Cooperative SWIPT MIMO-NOMA for reliable THz 6G communications," Network **2**, 257 (2022).
23. A. Kumar, M. Gupta, P. Pitchappa, *et al.*, "Phototunable chip-scale topological photonics: 160 Gbps waveguide and demultiplexer for THz 6G communication," Nat. Commun. **13**, 5404 (2022).
24. Y. Huang, Z. Yao, C. He, *et al.*, "Terahertz surface and interface emission spectroscopy for advanced materials," J. Phys. Con. Mat. **31**, 153001 (2019).
25. S. Li, J. Yang, H. Zhao, *et al.*, "Terahertz time-domain spectroscopy and quantitative analysis of metal gluconates," Appl. Spec. **69**, 52 (2015).
26. J. G. Han, "Probing negative refractive index of metamaterials by terahertz time-domain spectroscopy," Opt. Express **16**, 1354 (2008).
27. K. J. Tielrooij, D. Paparo, L. Piatkowski, *et al.*, "Dielectric relaxation dynamics of water in model membranes probed by terahertz spectroscopy," Biophys. J. **97**, 2484 (2009).
28. J. Q. Zhang, Y. Y. Yan, H. W. Zhao, *et al.*, "Water hydration of polyethylene glycol dimethyl ether," J. Chem. Phys. **158**, 204302 (2023).
29. J. Q. Zhang, L. Y. Liu, Y. Chen, *et al.*, "Water dynamics in the hydration shell of amphiphilic macromolecules," J. Phys. Chem. B **123**, 2971 (2019).
30. J. Q. Zhang, Y. Y. Yan, B. Wang, *et al.*, "Water dynamics in the hydration shell of hyper-branched poly-ethylenimine," Phys. Chem. Chem. Phys. **24**, 18393 (2022).
31. D. E. Rosenfeld and C. A. Schmuttenmaer, "Dynamics of water confined within reverse micelles," J. Phys. Chem. B **110**, 14304 (2006).
32. M. D. Fayer, "Water in a crowd," Physiology **26**, 381 (2011).
33. K. Shiraga, A. Adachi, M. Nakamura, *et al.*, "Characterization of the hydrogen-bond network of water around sucrose and trehalose: microwave and terahertz spectroscopic study," J. Chem. Phys. **146**, 105102 (2017).
34. J. R. Hu, H. Yamahara, Z. Q. Liao, *et al.*, "Characterization of hydrogen bond network of waters around polyethylene glycol by broadband dielectric spectroscopy," Appl. Phys. Lett. **120**, 023702 (2022).